Chapter

Correlation between Structure, Electrical, and Magnetic Properties of Some Alkali-Oxide Materials

Amira Marzouki, Ameni Brahmia, Riadh Marzouki, Mosbah Jemmali, Ismat H. Ali and Mohamed Faouzi Zid

Abstract

In this chapter, the correlation between structure and electrical properties of $Na_2MP_{1.5}As_{0.5}O_7$ (M^{II} = Co and Cu) are treated. The structural study shows that the cobalt and copper isotype materials can be crystallized in the tetragonal and monoclinic systems, respectively. The electrical study using impedance spectroscopy technique showed that these mixed diphosphate diarsenates are fast electrical conductors; however, the cobalt material exhibited more conductive property than the copper compound. In addition, the powder perovskite manganites $La_{0.7}M_{0.2}M'_{0.1}MnO_3$ (M = Sr, Ba and M' = Na, Ag and K) have been prepared using the conventional solid-state reaction. The structural, magnetic, and magnetocaloric properties of these perovskite manganites compounds were studied extensively by means of X-ray powder diffraction (XRD) and magnetic measurements. These samples were crystallized in the distorted rhombohedral system with R3c space group. The variation of magnetization (M) vs. temperature (T) reveals that all compounds exhibit a second-order ferromagnetic to paramagnetic phase transition in the vicinity of the Curie temperature (TC). A maximum magnetic entropy change, $\Delta S_M{}^{Max}$, of 4.07 J kg^{-1} K^{-1} around 345 K was obtained in $La_{0.7}Sr_{0.2}Na_{0.1}MnO_3$ sample upon a magnetic field change of 5 T. The $\Delta S_M{}^{Max}$ values of $La_{0.7}Ba_{0.2}M'_{0.1}MnO_3$ are smaller in magnitude compared to $La_{0.7}Sr_{0.2}M'_{0.1}MnO_3$ samples and occur at lower temperatures.

Keywords: diphosphate-diarsenate, crystal structure, electrical properties, perovskite, magnetic materials, magnetocaloric effect

1. Introduction

The exploration of new alkali-based materials, especially Na-ion compounds, has become an area of intense activity [1–3]. In fact, these materials have the potential to replace lithium-based cathodes in the new generation of batteries. This trend can be explained by the global increase in demand for lithium and its toxicity compared to the low cost of sodium and its abundance in nature [4].

The two main methods of developing new cathodes, which are currently being explored, are either by researching new crystalline materials or by improving known materials by improving their electrical properties and electrochemical performance. In either case, crystallography remains the key to the development of these electrochemical systems as a determination of crystal structure and ion transport followed by electrochemical properties.

In this context, the exploration and investigation of phosphates, arsenates, and molybdates of transition metals and monovalent cations (Li, Na, K, Ag, etc.) have a promising field for various applications: electrical, piezoelectric processes, ferroelectric, magnetic, catalytic [5, 6]. Moreover, taking into account their remarkable structural richness, in particular the melilite structure [7], the olivine structure [8], and the sodium super ionic conductor (NaSICON) structure [9], these materials show several interesting physical properties, in particular, the ionic conduction and ion exchange [8, 9]. Many sodium-based materials have recently been prepared and tested for their electrical and/or electrochemical properties, including $Na_2CoP_2O_7$ [10], $LiCoAsO_4$ [11], $Na_{1.86}Fe_3(PO_4)_3$ [12], etc. These physicochemical properties are linked on the one hand to their structural wealth and on the other hand to the degree of openness of their anionic frameworks which can be dense, open, or microporous.

Thus, the investigation of this type of material requires a good correlation between crystal structure and electrical properties taking into account factors influencing the electrical conductivity such as porosity and the temperature range of stability of the crystal structure of the sample. In this chapter, the first part comprises a structural study of alkali metals (especially Na elements) transition metals (Co, Cu) phosphates-arsenates and their correlations with electrical properties.

On the other hand, alkaline atoms have an electronic procession, composed of a set of inert internal layers, having the structure of a rare gas, and an additional electron, or valence electron, which orbiting an s-type orbital. The study of ionization potentials shows that this electron is easily torn off, the heavier the atom is the lesser the energy is required for ionization. The chemistry of alkali metals is essentially constituted by the study of the transition to the ionized state M^+ and by the properties of this ion. Most alkaline compounds, therefore, have a purely ionic structure; this peculiarity, together with the fact that the most stable ionic edifices are constituted by ions of similar volume, makes it possible to predict that as a general rule hydrides, nitrides, carbides, and simple oxides, that is to say compounds possessing fairly small anions, will be all the more stable the lighter the alkali metal, while the salts corresponding to large anions, peroxides $(O—O)^{2-}$, superoxides $(O—O)^-$, oxacids, and halides will be more stable with heavy alkali metals.

The dangers of the impact of synthetic refrigerants on the environment are central to the global ecological scene. Global warming, by its complexity and magnitude, poses several challenges to the ecological future of the earth. One of the solutions proposed to slow down this process is to reduce the production of greenhouse gases. While demand is growing, the areas of refrigeration and air conditioning are trying to renew themselves to meet the new ecological requirements. Such developments will lead to new technologies applicable to domestic and industrial uses of microtechnologies, HVAC systems refrigerators, heat pumps and affecting the automotive, railway, aeronautical, and aerospace industries. Magnetocaloric cooling (MCE) is a possible solution and becomes a promising attempt. Magnetic refrigeration is a technology that relies on the magnetocaloric effect, similar to compressibility refrigerant for gas refrigeration.

The magnetocaloric effect being present in all magnetic substances gives a large field of research activity to find active materials suitable for every utility [13, 14]. Gadolinium is the reference material for magnetic cold at room temperature. This

element also has the advantage of being an easy compound to obtain through its purity. It finds its technological development, thanks to the ease of implementation reflected by its high ductility and suitability. This is why it is used in most current magnetic refrigeration devices at room temperature. However, its prohibitive price (up to 3500 €/kg) and its limited reserves preclude it from possible magnetocooling materials for consumer applications. It is, therefore, important to find another magnetocaloric material. Manganese is an energetically clean alternative to address this problem and may be potential material for magnetic refrigeration.

The compounds $LnMnO_3$, Ln_2MnO_4 (where Ln is a rare earth) are antiferromagnetic insulators. The partial substitution of Ln^{3+} by a divalent element A^{2+} (A^{2+} = Ca^{2+}; Sr^{2+}; Ba^{2+}; Pb^{2+} ...), monovalent A^+ (A^+ = Ag^+, Na^+, K^+ ...), trivalent A^{3+} (A^{3+} = Nd^{3+}, Sm^{3+}, Pr^{3+} ...), or a gap in $Ln_{1-x}A_xMnO_3$ results in oxidation or partial reduction of Mn^{3+}/Mn^{4+} ions, a structural transition (cubic ↔ rhombohedral ↔ orthorhombic) and an antiferromagnetic order change T_N = 125 K in $LaMnO_3$) ferromagnetic with Tc > 360 K depending on the composition [15–22].

The manganese oxides, which we are interested in given the importance of their electrical and magnetic properties [23, 24], crystallize in a perovskite-like structure. For this structure, of general formula ABO_3, the Bravais network of sites B (octahedral site), whose species are generally transition cations (Mn^{3+}, Mn^{4+}, Ti^{4+}, Al^{3+} ...) occupying the eight vertices of the cube, is simple cubic. Oxygen ions occupy the midpoints of the ridges, and species A in coordination 12 (cuboctahedral site) occupying the center of the cube are alkaline ions (K^+, Na^+, Ag^+ ...). Alkaline earth (Sr^{2+}, Ca^{2+}, Pb^{2+} ...) or rare earths (La^{3+}, Pr^{3+}, Nd^{3+} ...). Site B is, therefore, occupied by an ion of octahedral coordination, manganese in the case of manganites, thus forming the MnO_6 octahedra (**Figure 1**(**a**) and (**b**)).

It should be noted that the cations A and B must allow the electroneutrality of the compound; that is, the sum of the charges of the cations A and B must be equal to the total charge of the anions. Three types of ternary oxides can be found: cation A is monovalent (A^+ B^{5+} $O^{2-}{}_3$), bivalent (A^{2+} B^{4+} $O^{2-}{}_3$), or trivalent (A^{3+} B^{3+} $O^{2-}{}_3$).

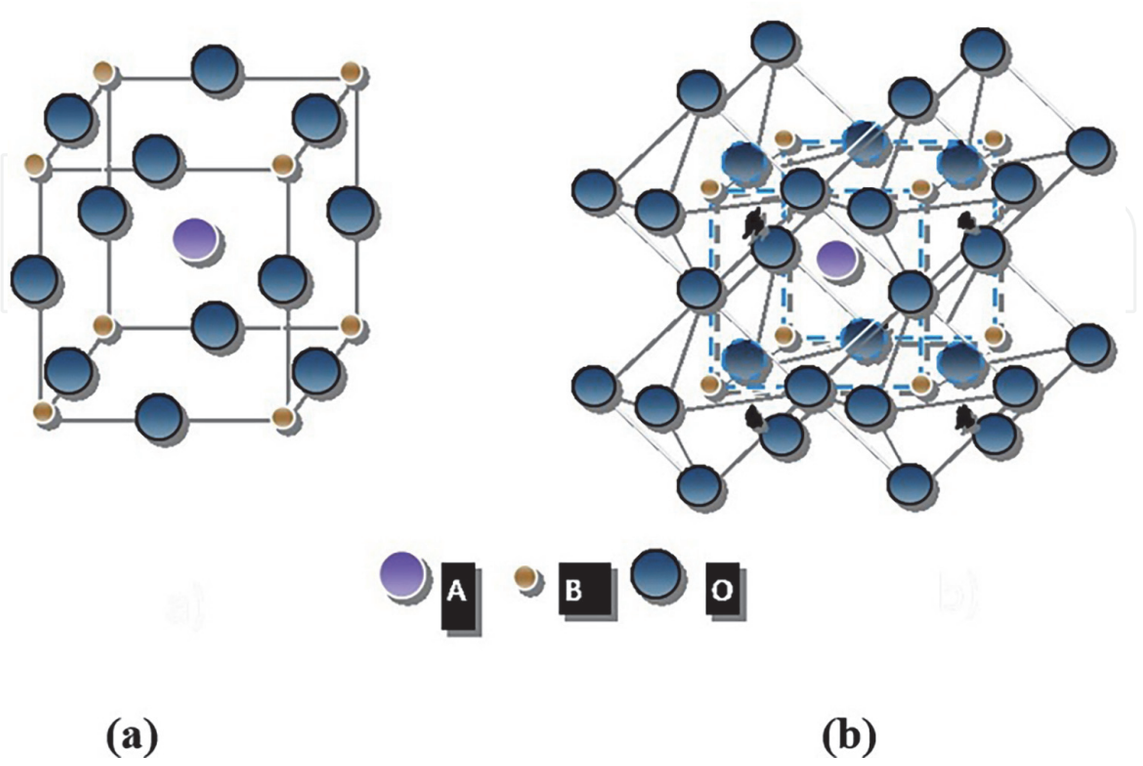

Figure 1.
Unit cell ABO_3 (a), octahedral environment of species B and (b) cuboctahedral environment of species A.

2. Structure, characterization, and electrical properties of $Na_2MP_{1.5}As_{0.5}O_7$ (M^{II} = Co and Cu).

2.1 Structural characterizations

The X-ray powder diffractograms were recorded in the range 10–70° at 20°C with 0.02° step (**Figures 2** and **3**). GSAS software [25] using Rietveld method was used to confirm the crystallinity and purity of the obtained powders. The final reliability factors are Rp = 1.4%, Rwp = 1.9%, and Rp = 5.4%, Rwp = 6.9%, of the Co and Cu samples, respectively.

In this case, the difference between the two diffractograms is noticeable. Indeed, the $Na_2CoP_{1.5}As_{0.5}O_7$ [26] material crystallizes in the tetragonal system of the space group P42/mnm with the unit cell parameters a = 7.764 (3) Å; c = 10.385 (3) Å.

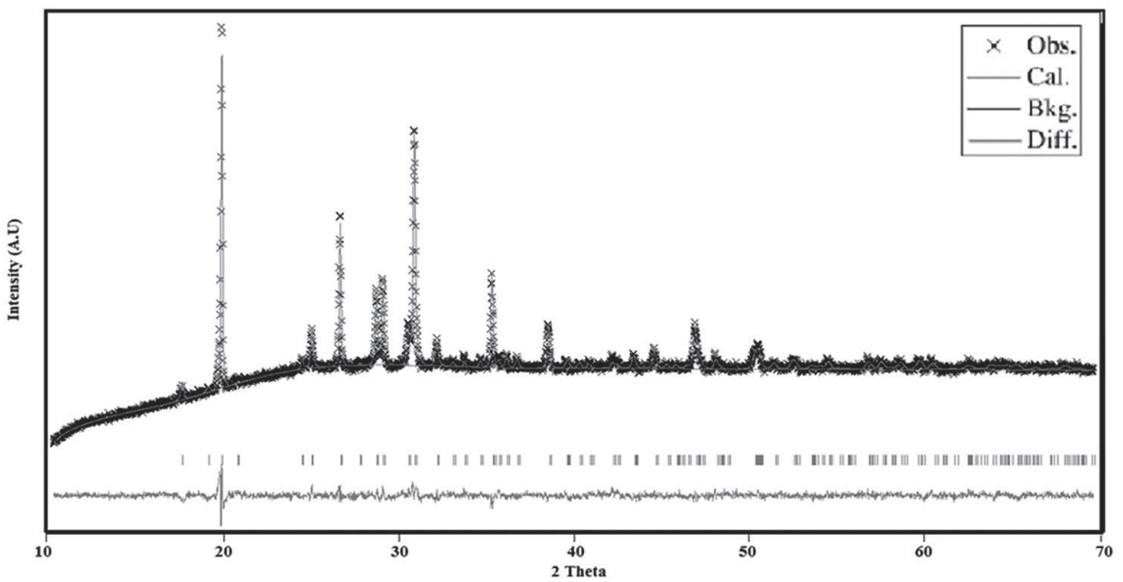

Figure 2.
Rietveld refinement pattern of $Na_2CoP_{1.5}As_{0.5}O_7$ powder.

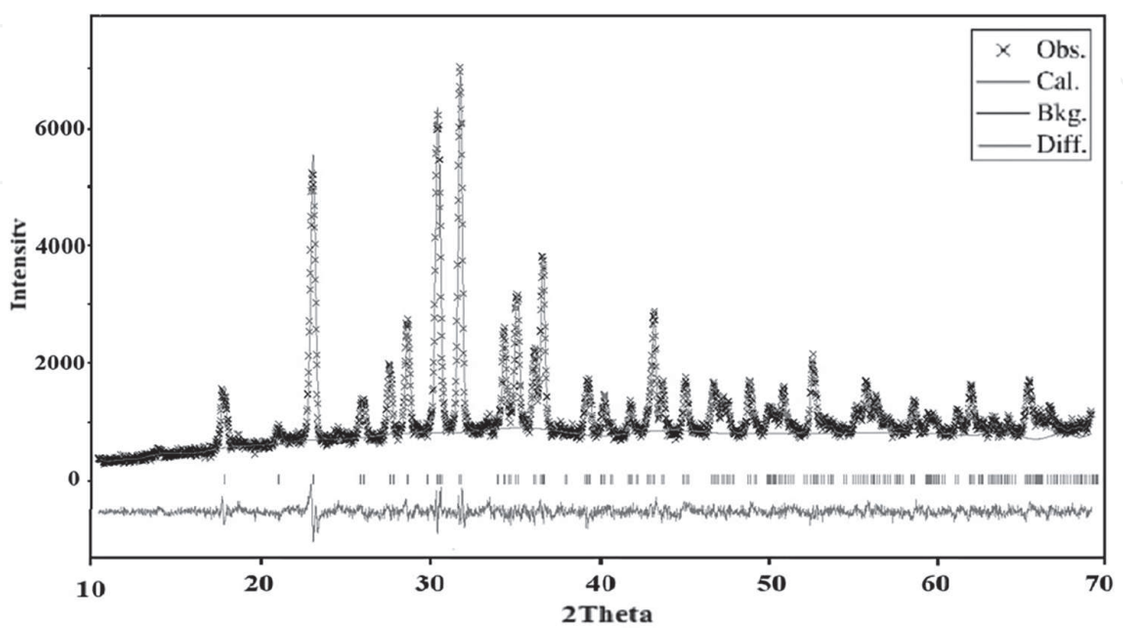

Figure 3.
Rietveld refinement pattern of $Na_2CuP_{1.5}As_{0.5}O_7$ powder.

While the compound $Na_2CuP_{1.5}As_{0.5}O_7$ [27] crystallizes in the monoclinic system of the C2/c space group with the unit cell parameters a = 14.798 (2) Å; b = 5.729 (3) Å; c = 8.075 (2) Å; β = 115.00 (3)°.

In fact, the structural unit of the compound $Na_2CoP_{1.5}As_{0.5}O_7$ is formed by a site occupied by a cobalt atom, a site occupied by a phosphorus atom partially substituted by arsenic, two sites for the sodium atoms and three sites for the sodium atoms ten oxygen atoms. The asymmetric unit is shown in **Figure 4**.

(i) −y + 1/2, x − 1/2, −z + 1/2; (ii) −x + 1, −y, z; (iii) y + 1/2, −x + 1/2, −z + 1/2].

The projection of the structure in the b direction (**Figure 5**) illustrates the layered nature of the anionic framework with two alternating orientations of anion

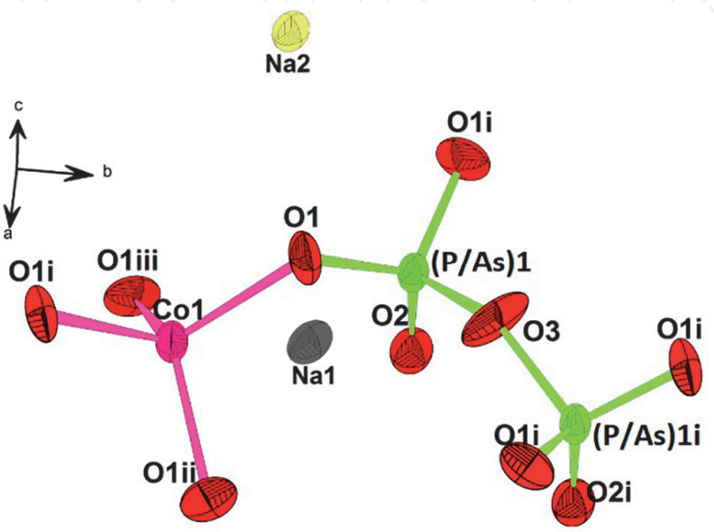

Figure 4.
Structural unit of $Na_2CoP_{1.5}As_{0.5}O_7$ with atom labeling scheme.

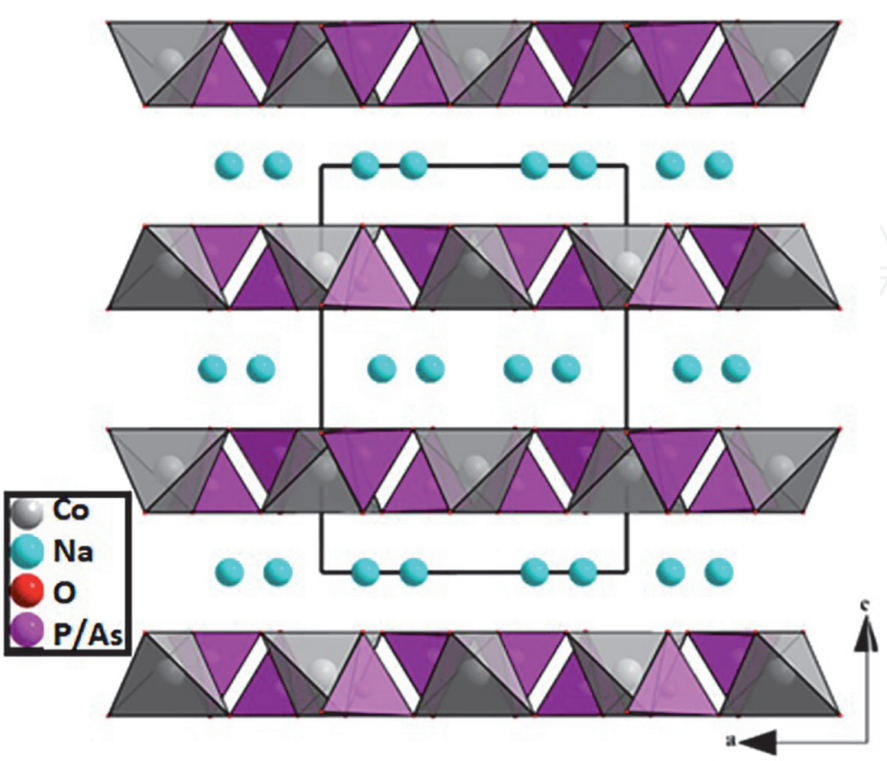

Figure 5.
Projection of the $Na_2CoP_{1.5}As_{0.5}O_7$ along b *direction.*

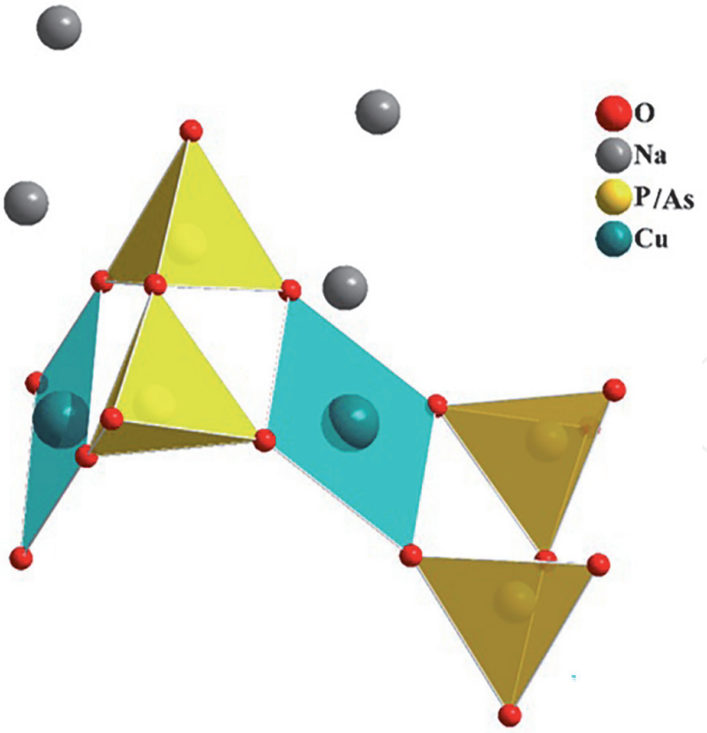

Figure 6.
Structural unit projection of $Na_2CuP_{1.5}As_{0.5}O_7$.

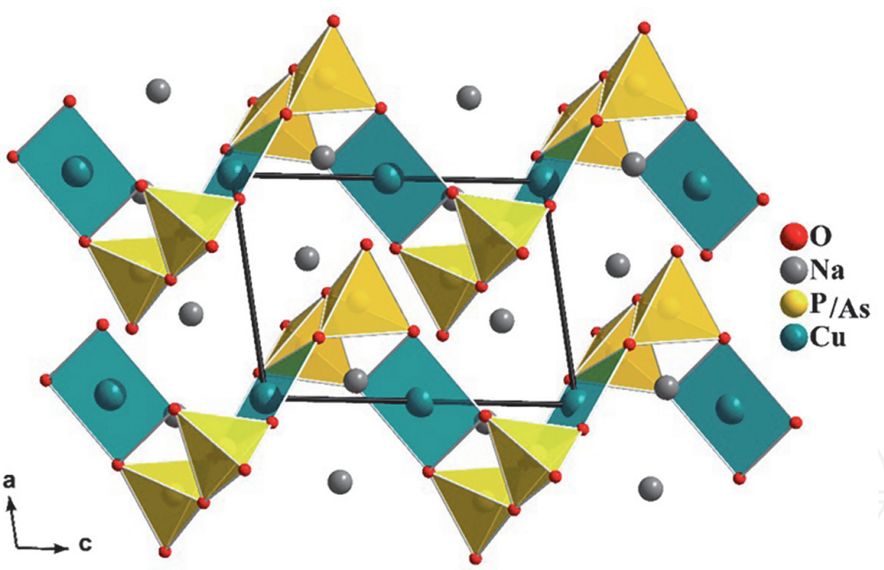

Figure 7.
Structure projection of $Na_2CuP_{1.5}As_{0.5}O_7$ in the ac plane showing the chain arrangement.

sheets $[Co(P/As)_2O_7]^{2-}$ per unit cell parallel to the *ab* plane where sodium cations are sandwiched between layers. Compared to $Na_2CoP_2O_7$ [28] crystal structure, the substitution of the phosphorus ions by arsenic cations decreases the size of the interlayer space and decreases in binding Na—O distance.

On the other hand, the structural unit of $Na_2CuP_{1.5}As_{0.5}O_7$ (**Figure 6**) contains two P_2O_7 units connected by the corner with two CuO_4 with square plane geometry. The charge neutrality of the structural unit is ensured by four sodium ions.

The $Cu_2P_4O_{15}$ groups of the structural unit are linked by oxygen peaks to give infinite chains, wavy sawtooth in the [001] direction (**Figure 7**). Na^+ ions are located in the inter-chain space.

2.2 Electrical study of $Na_2CoP_{1.5}As_{0.5}O_7$

The electrical properties of the cobalt compound were studied using complex impedance spectroscopy [29] in the temperature range from 240 to 360°C after stabilization at each step of 30°C between 1 Hz and 13 MHz frequency range. The electrical parameters are concluded using the conventional electrical circuit: R//CPE-R//CPE, where R_{est} is a resistance and CPE is a constant phase element:

The electrical parameters are summarized in **Table 1**.

The electrical measurements show that the electrical conductivity of $Na_2CoP_{1.5}As_{0.5}O_7$ increases from 4.0×10^{-6} S cm^{-1} at 240°C to 3.69×10^{-5} S cm^{-1} at 360°C. On the other hand, the activation energy which follows Arrhenius' law is 0.56 eV.

2.3 Electrical study of $Na_2CuP_{1.5}As_{0.5}O_7$

The $Na_2CuP_{1.5}As_{0.5}O_7$ sample was sintered at 550°C for 2 h with 5°C/min of heating and cooling. The relative density of the obtained pellet is D = 88%. Electrical measurements in the temperature range of 260–380°C were performed using complex impedance spectroscopy. The recorded spectra are shown in **Figure 8**.

The best refinements of impedance spectra were obtained when using a conventional electrical circuit Rg//CPEg-Rgb//CPEgb.

T (°C)	R_{total} (10^5 Ω)	σ (10^{-5} S cm^{-1})	σ_d (10^{-4} S cm^{-1})
240	2.356	0.40	0.188
270	1.077	0.88	0.414
300	0.569	1.68	0.791
330	0.349	2.74	1.294
360	0.259	3.69	1.736

Table 1.
Results of electrical parameters of $Na_2CoP_{1.5}As_{0.5}O_7$.

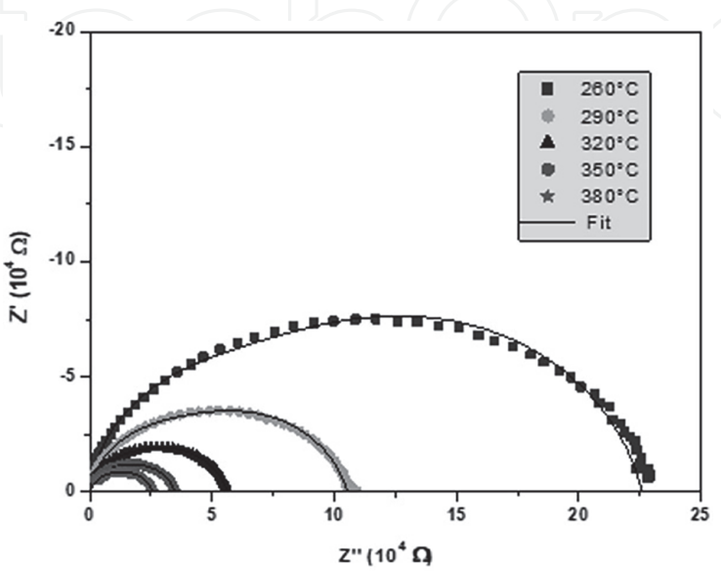

Figure 8.
Impedance spectra of $Na_2CuP_{1.5}As_{0.5}O_7$ recorded at 240–360°C.

T (°C)	Rt (10^4 Ω)	ρt (10^4 Ω cm)	σ (10^{-5} S cm^{-1})	σ_d (10^{-5} S cm^{-1})
260	22.58	28.58	0.35	1.59
290	10.52	13.32	0.75	3.41
320	5.61	7.10	1.41	6.41
350	3.47	4.39	2.28	10.36
380	2.52	3.19	3.13	14.23

Table 2.
Results of electrical parameters of $Na_2CuP_{1.5}As_{0.5}O_7$.

The values of the electrical parameters calculated at different temperatures are presented in **Table 2**.

The conductivity of $Na_2CuP_{1.5}As_{0.5}O_7$ (**Table 2**) increase from 0.35×10^{-5} S cm^{-1} at 260°C to 3.13×10^{-5} S cm^{-1} at 380°C. On the other hand, the porosity of 12% of our sample prompted us to estimate the conductivity values of the fully dense sample of $Na_2CuP_{1.5}As_{0.5}O_7$ using the empirical formula proposed by Langlois and Couret [30].

Taking into account the porosity factor P = 0.12, the conductivity value of the dense material will be $\sigma_d = (4\sigma/0.88)$. The conductivity values of a dense sample, calculated at different temperatures, are summarized in **Table 2**. In this case, the experimental conductivity of 3.5×10^{-6} S cm^{-1} corresponds to the corrected value of 1.59×10^{-5} S cm^{-1} to 260°C.

The activation energy calculated from the slope of the linear curve $Ln(\sigma \times T) = f(1000/T)$ is linear (**Figure 9**), with a slope that gives the value of Ea = 0.60 eV, satisfying Arrhenius law $Ln\sigma T = Ln\sigma_0 - Ea/kT$ (k = Boltzmann constant).

The electrical study shows that the activation energy decreases for $Na_2CuP_{1.5}As_{0.5}O_7$ compared to that of $Na_2CuP_2O_7$ [27], i.e., 0.60 eV and 0.89 eV, respectively. Therefore, the effect of P/As substitution increases the electrical conductivity of the parent phase $Na_2CuP_2O_7$ at a lower temperature [31]. Overall, a comparison of the conductivity values of the material studied $Na_2CuP_{1.5}As_{0.5}O_7$ (at T = 350°C, σ_d = 88% = 2.28×10^{-5} S cm^{-1}; $\sigma_d = 2.28 \times 10^{-4}$ S cm^{-1} and Ea = 0.60 eV) with those found in the literature shows that our material can be classified as fast ionic conductors.

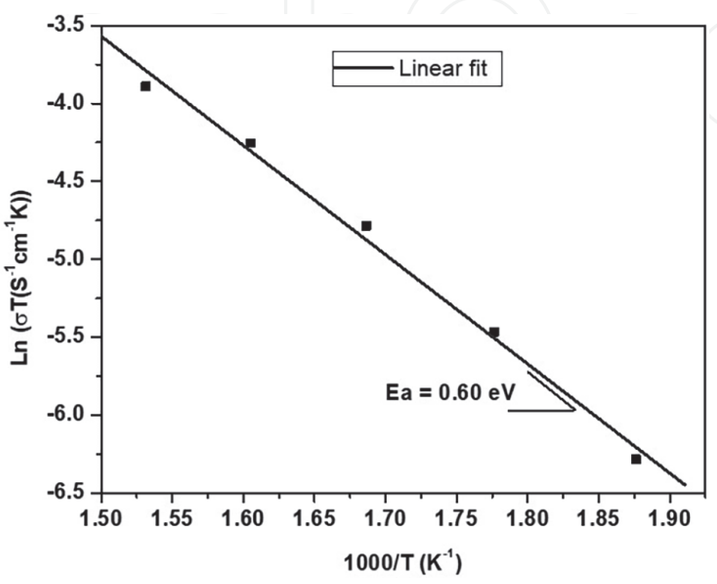

Figure 9.
Arrhenius plot of conductivity of the $Na_2CuP_{1.5}As_{0.5}O_7$ sample.

3. Structure, magnetic, and magnetocaloric of $La_{0.7}Sr_{0.2}K_{0.1}MnO_3$ and $La_{0.7}Ba_{0.2}Na_{0.1}MnO_3$ compounds

3.1 Structural characterization

Before proceeding with the magnetic study, it was necessary to ascertain the structure of the materials. Using the X-ray diffraction technique, it was possible to confirm that all the samples analyzed in this work have only one type of structure (single-phase) and that they corresponded to the given stoichiometry. The samples were reduced to powdered form, with a grinding time of 2 min, which was sufficient to obtain the random effect of orienting the structures without destroying them.

To check the nature and purity of the synthetic products, X-ray diffraction patterns were recorded at room temperature using the Panalytical X'Pert PRO diffractometer which is equipped with a copper anticathode ($\lambda K\alpha 1$ = 1.54056 Å, $\lambda K\alpha 2$ = 1.54439 Å) and provides good quality diffractograms.

Figure 10 presents the experimental X-ray diffraction spectra of $La_{0.7}Sr_{0.2}Na_{0.1}MnO_3$ compound refined via the WinPlotr graphical interface of FullProf_Suite which has been studied by W. Cheikh-Rouhou Koubaa et al. [32].

The Rietveld analysis of X-ray diffraction patterns shows that the $La_{0.7}Sr_{0.2}K_{0.1}MnO_3$ and $La_{0.7}Ba_{0.2}Na_{0.1}MnO_3$ compounds are single-phase and crystallize in the rhombohedral Th_2Zn_{17}-type structure (space group, R_3m).

Figure 11 shows the evolution of the unit cell volume compared to $\langle r_A \rangle$ for the two series. For $La_{0.7}Sr_{0.2}M_{0.1}MnO_3$ samples, an observed increase of $\langle r_A \rangle$ occurred with a slight decrease in the volume of the unit cell from 352.5 Å for *M* = Na to 351.1 Å for *M* = K. While in the compounds $La_{0.7}Ba_{0.2}M_{0.1}MnO_3$, the evolution of unit cells is rather governed by $\langle r_A \rangle$ than by σ^2 observed increase in unit cell volume. It should be noted that, although the ionic radius of site A and the size of the mismatch are similar for both samples, $La_{0.7}Sr_{0.2}K_{0.1}MnO_3$ and $La_{0.7}Ba_{0.2}Na_{0.1}MnO_3$, the unit cell volume has different values. This behavior highlights the effects of the difference in electronegativity between the A-site ions in our compounds [33]. With increasing $\langle r_A \rangle$, the Mn—O—Mn binding angle decreases from 166.7° for sample $La_{0.7}Sr_{0.2}Na_{0.1}MnO_3$ to 165.9° for the sample $La_{0.7}Ba_{0.2}Na_{0.1}MnO_3$. However, the Mn—O bond length increases from 1.957 Å to

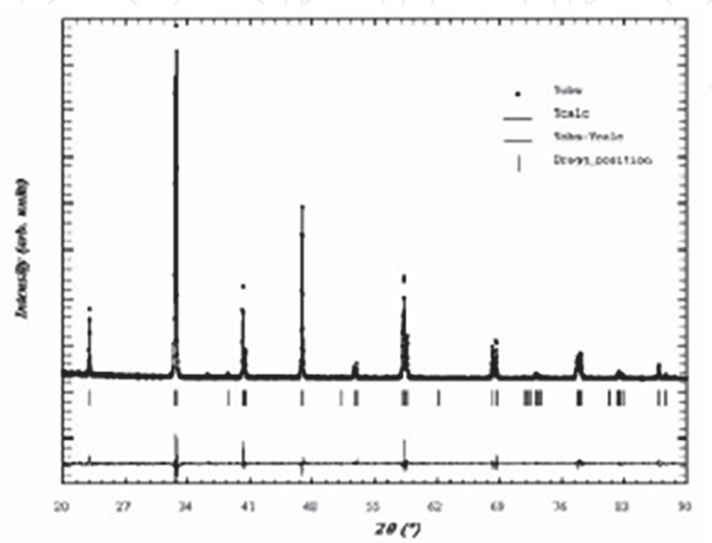

Figure 10.
X-ray diffraction patterns of $La_{0.7}Sr_{0.2}Na_{0.1}MnO_3$ sample.

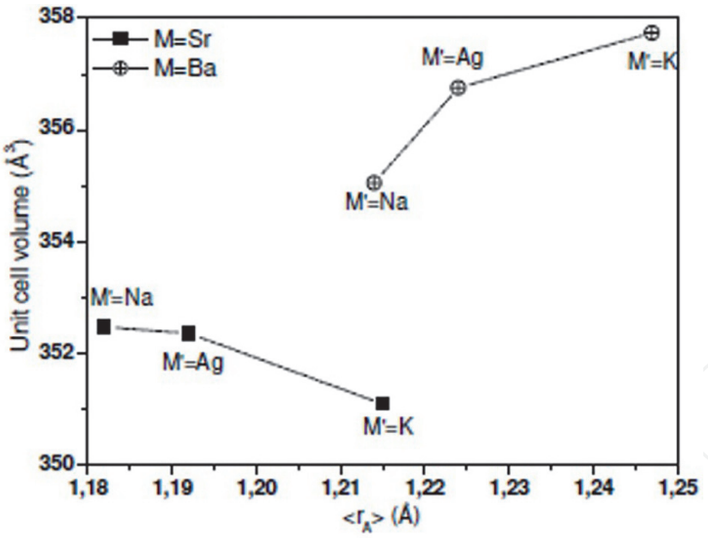

Figure 11.
Unit cell volume versus $\langle r_A \rangle$ for $La_{0.7}M_{0.2}M'_{0.1}MnO_3$ (M = Sr, Ba and M' = Na, Ag and K) samples.

1.968 Å, which influences the dual force of exchange. Effects of monovalent doping on the structural, magnetic, and magnetocaloric properties in $La_{0.7}M_{0.2}M'_{0.1}MnO_3$ manganese oxides (M = Sr, Ba and M' = Na, Ag, K) has been studied to control the value evaluation of magnetic entropy and cooling capacity.

3.2 Study of magnetic properties

The magnetic behaviors are subjected to two variables, which are the temperature and the applied magnetic field. It is possible to control these two factors experimentally and, thus, to keep one constant while studying the influence of the other on the magnetization M. The magnetic measurements were carried out on the two magnetometers BS2 and BS1 of the NEEL Institute used in the low/high-temperature configuration. The evolution of the magnetization as a function of the temperature and of the M(H, T) field was carried out on either side of the Curie temperature for each compound. The temperature of transition from the ferromagnetic state to the paramagnetic state was determined from the thermomagnetic curve M(T). TC corresponds to the minimum value of (dM/dT). The change in magnetic entropy was evaluated from the M(H, T) matrix based on the corresponding Maxwell equation.

Magnetic measurements of these compounds $La_{0.7}Sr_{0.2}K_{0.1}MnO_3$ and $La_{0.7}Ba_{0.2}Na_{0.1}MnO_3$ as a function of temperature in the temperature range 20–350 K under an applied magnetic field of 50mT show that all substituted samples show a magnetic transition from paramagnetic to ferromagnetic with decreasing temperature, as shown in **Figure 12**.

Figure 13 shows that the Curie temperature varies according to the ionic rays. It goes to lower values with $\langle r_A \rangle$ and varies from 340 K for $\langle r_A \rangle$ = 1.182 Å to 311.5 K for $\langle r_A \rangle$ = 1.247.

3.3 Study of magnetic properties under an applied magnetic field

In manganites, magnetism is essential of the localized type. A simple way to check, at low temperature, the ferromagnetic state, the fixed spin state, or the coexistence of a ferromagnetic and antiferromagnetic state of a sample, is to

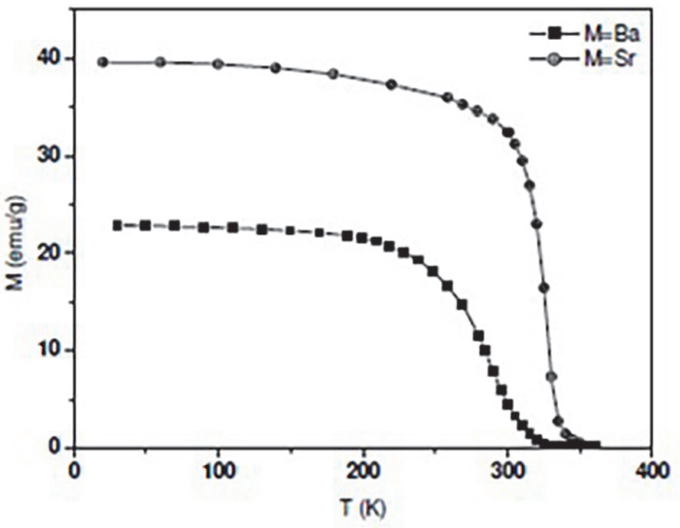

Figure 12.
Temperature dependence of the magnetization under an applied magnetic field 50 mT.

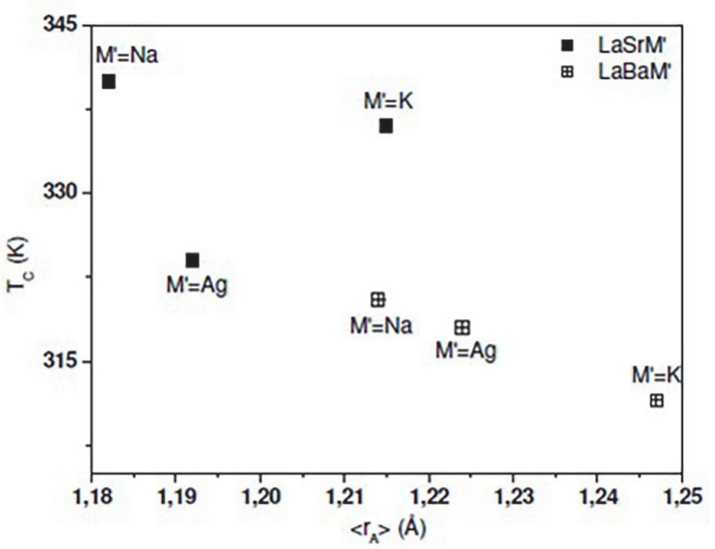

Figure 13.
Curie temperature versus $\langle r_A \rangle$ for $La_{0.7}M_{0.2}M'_{0.1}MnO_3$ (M = Sr, Ba and M' = Na, Ag and K) samples.

compare the value of the saturation magnetization with its calculated value assuming full alignment of the manganese spins of this compound. This procedure gives an estimate of the degree of alignment of the moments. For this, we present the study of the magnetic properties of these samples under an applied magnetic field up to the value of 7 tesla. As the study of the thermal variations of the magnetization under weak magnetic field (0.05 T) showed that the samples $Pr_{0.6-x}Eu_xSr_{0.4}MnO_3$ ($0.0 \leq x \leq 0.2$) present a magnetic transition as a function of the temperature, it is then interesting to specify the nature of the magnetic order at low temperatures. M'nassri et al. [34] performed magnetization measurements as a function of the magnetic field applied at various temperatures.

The difference observed between the compounds $La_{0.7}Sr_{0.2}K_{0.1}MnO_3$ and $La_{0.7}Ba_{0.2}Na_{0.1}MnO_3$ is fully explained by the effects of the difference in electronegativity between the ions at site A for the two samples. The magnetization measurements as a function of the applied magnetic field up to 7 T at several temperatures confirmed the ferromagnetic behavior of these samples at low temperature, and the results are shown in **Figure 14**.

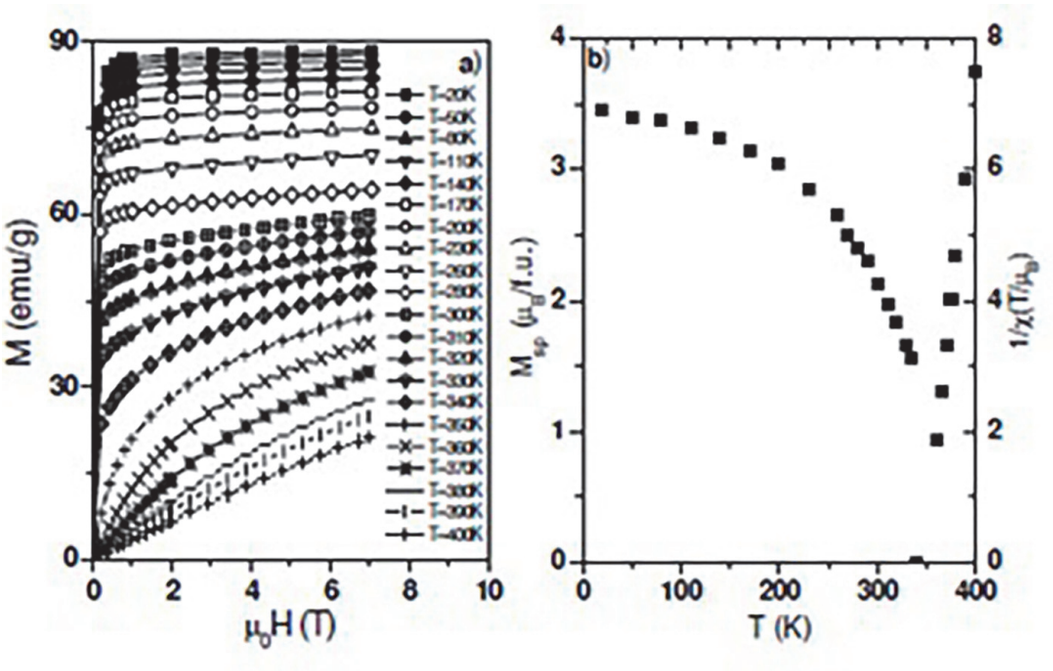

Figure 14.
(a) Isotherm magnetization curves M(H, T). (b) Temperature dependence of the spontaneous magnetization Msp and 1/χ for $La_{0.7}Sr_{0.2}Na_{0.1}MnO_3$ sample.

The authors show that below TC, the magnetization M increases strongly with the magnetic field applied for H < 0.5 T then saturates above 1 T. The saturation magnet changes to higher values as the temperature decreases. This result confirms the ferromagnetic behavior of our sample at low temperature. **Figure 14b** shows the temperature dependence of the spontaneous magnetization Msp and 1/χ for the sample $La_{0.7}Sr_{0.2}Na_{0.1}MnO_3$. The experimental value of the spontaneous magnetization Msp(exp), deduced from the M(H) curves is 3.48 μB/Mn. The amplitude of the Msp(exp) is comparable to the theoretical value of 3.6 μB/mole calculated for full spin alignment. The critical exponent defined by.

$$\mathrm{Msp(T)} = \mathrm{Msp(0)[1–T/T_C]}^{\nu} \quad (1)$$

and deduced from the fit of the curve Msp(T) is 0.31, which confirms the ferromagnetic behavior of the samples from the group Cheikh-Rouhou team at low temperature

3.4 Magnetocaloric effect

Entropy is a measure of order in the magneto-thermodynamic system. High order is related to low entropy and vice versa. Dipoles, that is, electron spins, can take on different orientations. If these entities are oriented in the same direction in a paramagnetic material, a ferromagnetic or a diamagnetic material, the order and the magnetization are high. It is obvious that applying a magnetic field aligns the electronic spins and lowering the temperature (releasing energy from the system) also results in a more ordered arrangement. So the external magnetic field generates the stress parameter, while the magnetization determines the order parameter of such magnetic materials.

In order to obtain a maximum of information on the thermodynamic behavior and to observe the magnetocaloric effect in the manganites in the vicinity from

their magnetic transition temperature, we have studied the magnetocaloric behavior of the whole range of composition x.

After having studied magnetic measurements of magnetization as a function of temperature M(T) as well as magnetization as a function of the magnetic field at various temperature M(μ_0H, T), we have calculated, the magnetic entropy change ΔS_M of all our synthesized compounds as a function of temperature T and magnetic field H.

Based on the thermodynamic theory, magnetic entropy change is determined through the numerical integration of the magnetization isotherms, according to Maxwell's thermodynamic relation given by the following equation [34, 35]:

$$\Delta S_M(T, \Delta H) = \int_0^H \mu_0 \left(\frac{\partial M}{\partial T}\right)_{P,H} dH \tag{2}$$

$$\Delta S_M(T_i, \Delta H) = -\sum_j \frac{M_{i+1}(T_{i+1}, H_j) - M_i(T_i, H_j)}{T_{i+1} - T_i} \mu_0 \delta H_j \tag{3}$$

where M_i and M_{i+1} are the magnetization values measured at the H_i field and at temperatures T_i and T_{i+1}, respectively [35].

We have shown in **Figure 15**, the variations in entropy ($-\Delta S_M$) as a function of temperature for different magnetic fields applied for these $La_{0.7}Sr_{0.2}Na_{0.1}MnO_3$ and $La_{0.7}M_{0.2}M'_{0.1}MnO_3$ sample (*M* = Sr, Ba and M' = Na, Ag and K) system. These curves show that the entropy value ($-\Delta S_M$) varies with temperature and has a peak around the transition temperature TC. The sample $La_{0.7}Sr_{0.2}Na_{0.1}MnO_3$ shows the highest value of ΔS_M^{Max}, 4.07 J kg^{-1} K^{-1}, around 345 K. For the sample $La_{0.7}Ba_{0.2}Na_{0.1}MnO_3$, we observed an asymmetric broadening of the peak ΔS_M, which could be explained by a structural inhomogeneity. We can also notice that the magnetic and negative entropy for all our samples was due to the ferromagnetism encountered in these samples. The value of the entropy ($-\Delta S_M^{Max}$) was also observed to increase when the applied magnetic field increased. Although these ΔS_M^{Max} values in these samples are lower than those observed in Gd or Gd-based compounds, the ΔS_M^{Max} curves as a function of temperature are significantly wider.

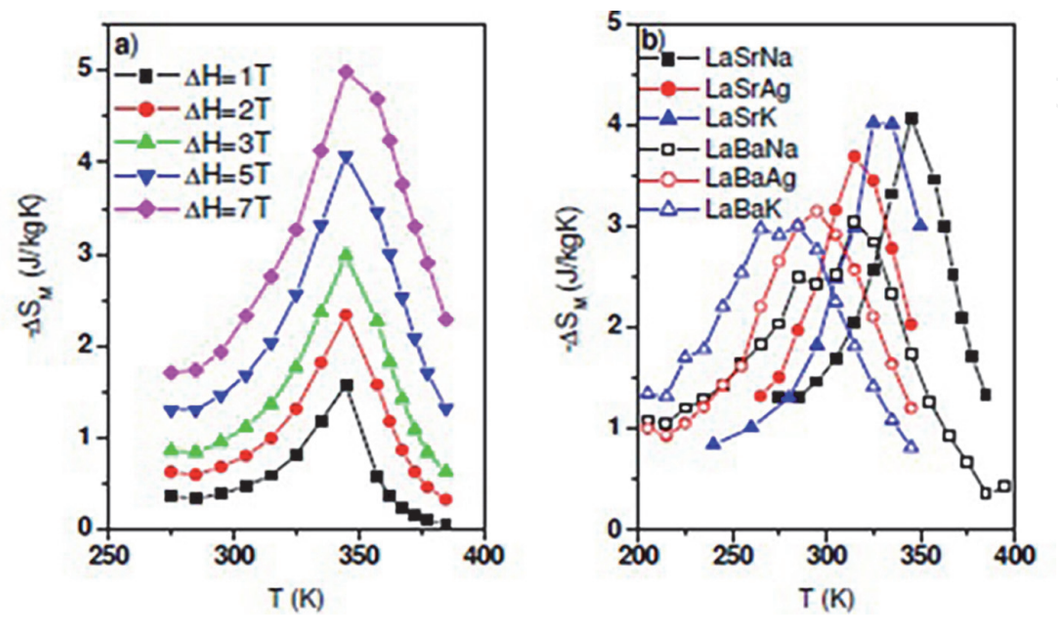

Figure 15.
*Magnetic entropy change $-\Delta S_M$ evolution versus temperature at (a) Several magnetic applied fields for $La_{0.7}Sr_{0.2}Na_{0.1}MnO_3$ sample (b) At 5 T for $La_{0.7}M_{0.2}M'_{0.1}MnO_3$ samples (*M = Sr, Ba and* M' = Na, Ag and K).*

This wider temperature range with a large change in magnetic entropy is useful for an ideal Ericsson refrigeration cycle. In addition, our samples are interesting in application as potential candidates in magnetic refrigeration because they are inexpensive, easier to manufacture, possess tunable T_C, and have high chemical resistance stability.

4. Conclusion

During our research on the investigation of new phosphates, arsenates of metals (Co, Cu) and alkali cations, we were able to isolate 2 crystalline phases. These compounds have shown remarkable structural diversity, even though they are isoformular. The synthesis method adopted was dry synthesis. In addition, P/As substitution showed conservation of structure in each material with variation in cation-oxygen distances. On the other hand, the effect of substitution is remarkable on the electrical properties. In fact, the sodium Co and Cu diphosphates-diarsenates are more conductive than the pure diphosphates. Alkaline atoms have an electronic procession, composed of a set of inert internal layers, having the structure of a rare gas, and an additional electron, or valence electron, which orbiting an s-type orbital. The magnetic and magnetocaloric study on the $La_{0.7}M_{0.2}M'_{0.1}MnO_3$ family shows that there is a Curie temperature in the vicinity of the room temperature and very high magnetic entropy values. We can conclude that these compounds are good candidates for magnetic refrigeration.

Author details

Amira Marzouki[1], Ameni Brahmia[2,3], Riadh Marzouki[2,4]*, Mosbah Jemmali[4], Ismat H. Ali[2] and Mohamed Faouzi Zid[5]

1 Laboratory of Signal Image and Energy Mastery, Engineering National Higher School of Tunis, Tunis, Tunisia

2 Chemistry Department, College of Science, King Khalid University, Abha, Saudi Arabia

3 Laboratoire des Materiaux et de l'Environnement pour le Developpement Durable, LR18ES10, University of Tunis El Manar, Tunisia

4 Faculty of Science, LSME, University of Sfax, Sfax, Tunisia

5 Faculty of Sciences of Tunis, Laboratory of Materials, Crystallochemistry and Applied Thermodynamics, University of Tunis El Manar, Tunisia

*Address all correspondence to: rmarzouki@kku.edu.sa

References

[1] Brian LE, Nazar F. Sodium and sodium-ion energy storage batteries. Current Opinion in Solid State & Materials Science. 2012;**16**:168-177

[2] Shakoor RA, Seo DH, Kim H, Park YU, Kim J, Kim SW, et al. A combined first principles and experimental study on $Na_3V_2(PO_4)_2F_3$ for rechargeable Na batteries. Journal of Materials Chemistry. 2012;**22**:20535

[3] Kim H, Shakoor RA, Park C, Yeon Lim S, Kim JS, Jo YN, et al. $Na_2FeP_2O_7$ as a positive electrode material for rechargeable aqueous sodium-ion batteries. Advanced Functional Materials. 2013;**23**:1147

[4] Peng Y, Yang L, Ju X, Liao B, Ye K, Li L, et al. A comprehensive investigation on the thermal and toxic hazards of large format lithium-ion batteries with $LiFePO_4$ cathode. Journal of Hazardous Materials. 2020;**381**:120916

[5] Goodenough JB, Hong HY-P, Kafalas JA. Fast Na^+ -ion transport in skeleton structures. Materials Research Bulletin. 1976;**11**:203-220

[6] Kanazawa T. Inorganic Phosphate Materials, Materials Science Monographs. Vol. 52. Amsterdam: Elsevier; 1989

[7] Erragh F, Boukhari A, Elouadi B, Holt EM. Crystal structures of two allotropic forms of $Na_2CoP_2O_7$. Journal of Crystallographic and Spectroscopic Research. 1991;**21**:321-326

[8] Padhi AK, Nanjundaswamy K, Goodenough JB. Phospho-olivines as positive-electrode materials for rechargeable lithium batteries. Journal of the Electrochemical Society. 1997; **144**(4):1188-1194

[9] Durif A. Crystal Chemistry of Condensed Phosphates. US: Springer; 1995

[10] Barpanda P, Lu J, Ye T, Kajiyama M, Chung S-C, Yabuuchi N, et al. A layerstructured $Na_2CoP_2O_7$ pyrophosphate cathode for sodium-ion batteries. RSC Advances. 2013;**3**: 3857-3860. DOI: 10.1039/C3RA23026K

[11] Satya Kishore MVVM, Varadaraju UV. Synthesis, characterization and electrochemical studies on $LiCoAsO_4$. Materials Research Bulletin. 2006;**41**: 601-607

[12] Essehli R, Ben Yahia H, Maher K, Sougrati MT, Abouimrane A, Park J-B, et al. Unveiling the sodium intercalation properties in $Na_{1.86}\square_{0.14}Fe_3(PO_4)_3$. Journal of Power Sources. 2016;**324**: 657-664

[13] Tishin AM, Spichkin YI. The Magnetocaloric Effect and Its Applications. Bristol: Institute of Physics Publishing; 2003

[14] Tegus O, Brück E, Buschow KHJ, de Boer FR. Transition-metal-based magnetic refrigerants for room-temperature applications. Nature. 2002; **415**:150

[15] Cherif K, Dhahri J, Dhahri E, Oumezzine M, Vincent H. Effect of indium substitution on structural, magnetic and magnetocaloric properties of $La_{0.5}Sm_{0.1}Sr_{0.4}Mn_{1-x}In_xO_3$ ($0 \leq x \leq 0.1$) manganites. Journal of Solid State Chemistry. 2002;**163**:466

[16] Tlili MT, Chihaoui N, Bejar M, Dhahri E, Valente MA, Hlil EK. Charge ordering analysis by electrical and dielectric measurements in $Ca_{2-x}Pr_xMnO_4$ (x = 0–0.2) compounds. Journal of Alloys and Compounds. 2011; **509**:6447

[17] Daoudi A, Le Flem G. Sur une série de solutions solides de formule $Ca_{2-x}Ln_xMnO_4$ (Ln = Pr, Nd, Sm, Eu,

Gd). Journal of Solid State Chemistry. 1972;**5**:57

[18] Takahashi J, Kamegashira N. Low-temperature structural phase transitions in rare earths substituted calcium manganese oxides [$Ca_{2-x}Ln_xMnO_4$, where Ln=Nd, Sm-Lu and Y]. Materials Research Bulletin. 1993;**28**:451

[19] Takahashi J, Kikuchi T, Satoh H, Kamegashira N. Phase transition of $Ca_{2-x}Sm_xMnO_4$ ($x < 0.5$). Journal of Alloys and Compounds. 1993;**192**:96

[20] Dhahri E, Guidara K, Cheikhrouhou A, Joubert JC, Pierre J. Monovalent effects on structural, magnetic and magnetoresistance properties in doped manganite oxides. Phase Transitions. 1998;**66**:99

[21] Teresa JMDE, Ibarra MR, Garcia J, Blasco J, Ritter C, Algarabel PA, et al. Spin-glass insulator state in $(Tb\text{-}La)_{2/3}Ca_{1/3}MnO_3$ perovskite. Physical Review Letters. 1996;**76**:3392

[22] Ju HL, Kwon C, Li Q, Greene RL, Venkatesan T. Magnetic anisotropy and strain states of (001) and (110) colossal magnetoresistance thin films. Applied Physics Letters. 1994;**65**:2108

[23] Ziese M. Extrinsic magnetotransport phenomena in ferromagnetic oxides. Reports on Progress in Physics. 2002; **65**:143

[24] Shankar KS, Kar S, Raychaudhuri AK, Subbanna GN. Fabrication of ordered array of nanowires of $La_{0.67}Ca_{0.33}MnO_3La_{0.67}Ca_{0.33}MnO_3$ (x=0.33)(x=0.33) in alumina templates with enhanced ferromagnetic transition temperature. Applied Physics Letters. 2003;**84**(6):993

[25] Larson AC, Von Dreele RB. General Structure Analysis System (GSAS). Report LAUR 86–748. Los Alamos, NM: Los Alamos National Laboratory; 2000

[26] Marzouki R, Ben Smida Y, Sonni M, Avdeev M, Zid MF. Synthesis, structure, electrical properties and Na^+ migration pathways of $Na_2CoP_{1.5}As_{0.5}O_7$. Journal of Solid State Chemistry. 2020;**285**: 121058

[27] ALQarni OSA, Marzouki R, Smida YB, Avdeev M, Alghamdi MM, Zid MF. Synthesis, electrical properties and Na+ migration pathways of $Na_2CuP_{1.5}As_{0.5}O_7$. PRO. 2020;**8**:305

[28] MacDonald JR. Impedance Spectroscopy. New York: Wiley; 1987

[29] Sanz F, Parada C, Rojo JM, Ruiz-Valero C, Saez-Puche R. Studies on tetragonal $Na_2CoP_2O_7$, a novel ionic conductor. Journal of Solid State Chemistry. 1999;**145**(2):604-611. DOI: 10.1006/jssc.1999.8249

[30] Langlois S, Couret F. Electrochemical measurements of mass transfer coefficients in a cell simulating tooth canals. Journal of Applied Electrochemistry. 1989;**19**:43

[31] Hafidi E, El Omari M, El Omari M, Bentayeb A, Bennazha J, El Maadi A, et al. Conductivity studies of some diphosphates with the general formula $A^I{}_2B^{II}P_2O_7$ by impedance spectroscopy. Arabian Journal of Chemistry. 2013;**6**: 253-263

[32] Cheikh-Rouhou Koubaaa W, Koubaaa M, Cheikhrouhou A. Effect of monovalent doping on the structural, magnetic and magnetocaloric properties in $La_{0.7}M_{0.2}M'_{0.1}MnO_3$ manganese oxides (M=Sr, Ba and M′=Na, Ag, K). Physics Procedia. 2009;**2**:989-996

[33] Koubaa WC, Koubaa M, Cheikhrouhou A. Structural, magnetotransport, and magnetocaloric properties of $La_{0.7}Sr_{0.3-x}Ag_xMnO_3$ perovskite manganites. Journal of Alloys and Compounds. 2008;**453**:42

[34] M'nassri R, Cheikhrouhou-Koubaa W, Koubaa M, Boudjada N, Cheikhrouhou A. Magnetic and magnetocaloric properties of $Pr_{0.6-x}Eu_xSr_{0.4}MnO_3$ manganese oxides. Solid State Communications. 2011; **151**:1579

[35] Mc Michael RD, Ritter JJ, Shull RD. Enhanced magnetocaloric effect in $Gd_3Ga_{5-x}Fe_xO_{12}$. Journal of Applied Physics. 1993;**73**:6946